

## Holocene climate variability in the Winter Rainfall Zone of South Africa

S. Weldeab et al.

# Holocene climate variability in the Winter Rainfall Zone of South Africa

S. Weldeab<sup>1</sup>, J.-B. W. Stuut<sup>2,3</sup>, R. R. Schneider<sup>4</sup>, and W. Siebel<sup>5</sup>

<sup>1</sup>Department of Earth Science, University of California, Santa Barbara, CA 93106-9630, USA

<sup>2</sup>NIOZ, Royal Netherlands Institute for Sea Research, Texel, The Netherlands

<sup>3</sup>MARUM, Center for Marine Environmental Sciences, University of Bremen, Bremen, Germany

<sup>4</sup>Institute of Geosciences, University of Kiel, Kiel, Germany

<sup>5</sup>Department of Geosciences, University of Tübingen, Tübingen, Germany

Received: 11 March 2013 – Accepted: 27 March 2013 – Published: 7 May 2013

Correspondence to: S. Weldeab (weldeab@geol.ucsb.edu)

Published by Copernicus Publications on behalf of the European Geosciences Union.

Title Page

Abstract

Introduction

Conclusions

References

Tables

Figures

⏪

⏩

◀

▶

Back

Close

Full Screen / Esc

Printer-friendly Version

Interactive Discussion

## Abstract

We established a multi-proxy time series comprising analyses of major elements in bulk sediments, Sr and Nd isotopes and grain size of terrigenous fraction, and  $\delta^{18}\text{O}$  and  $\delta^{13}\text{C}$  in tests of *Neogloboquadrina pachyderma* (sinistral) from a marine sediment sequence recovered off the Orange River. The records reveal coherent patterns of variability that reflect changes in wind strength, precipitation over the river catchments, and upwelling of cold and nutrient-rich coastal waters off western South Africa. The wettest episode of the Holocene in the Winter Rainfall Zone (WRZ) of South Africa occurred during the “Little Ice Age” (700–100 yr BP). Wet phases were accompanied by strengthened coastal water upwellings, a decrease of Agulhas water leakage into the southern Atlantic, and a reduced dust incursion over Antarctica. A continuous aridification trend in the WRZ and a weakening of the southern Benguela Upwelling System (BUS) between 9000 and 5500 yr BP parallel with increase of dust deposition over Antarctica and an enhanced leakage of warm Agulhas water into the southeastern Atlantic. The temporal relationship between precipitation changes in the WRZ, the thermal state of the coastal surface water, and leakage of warm water in southern Atlantic, and variation of dust incursion over Antarctica suggests a causal link that most likely was related to latitudinal shifts of the Southern Hemisphere westerlies. Our results of the mid-Holocene time interval may serve as an analogue to a possible long-term consequence of the current and future southward shift of the westerlies that may result in a decline of rainfall over southwest Africa and a weakened upwelling with implication for phytoplankton productivity and fish stocks. Furthermore, warming of the coastal surface water as a result of warm Agulhas water incursion into the southern BUS may affect coastal fog formation that is critical as moisture source for the endemic flora of the Namaqualand.

## Holocene climate variability in the Winter Rainfall Zone of South Africa

S. Weldeab et al.

[Title Page](#)

[Abstract](#)

[Introduction](#)

[Conclusions](#)

[References](#)

[Tables](#)

[Figures](#)

[⏪](#)

[⏩](#)

[◀](#)

[▶](#)

[Back](#)

[Close](#)

[Full Screen / Esc](#)

[Printer-friendly Version](#)

[Interactive Discussion](#)



## 1 Introduction

Instrumental and modeling data indicate that the southward displacement of austral westerlies and increased amount of leakage of warm, saline Agulhas water into the southern Atlantic may have a negative impact on the Winter Rainfall Zone (WRZ) of South Africa and weaken the southern BUS (Blastoch et al., 2008, 2009; Lutjeharms et al., 2001; MacKellar et al., 2007; Hardman-Mountford et al., 2003). Paleoclimate records can provide insights that may help to assess the long-term impact of such ocean-atmosphere changes. However, conventional terrestrial climate archives such as lake and cave deposits are sparse in arid and semi-arid regions, limiting a dense spatio-temporal coverage and multi-proxy approach of climate reconstructions, a prerequisite to gaining a better understanding of regional climate variability and its link to large-scale atmosphere–ocean climate coupling. The coastal area of southwest Africa is located in the semi-arid ecosystem (MacKellar et al., 2007 and reference therein), and our knowledge of past climate variability so far has relied on a few low-resolved proxy records. The emergence of new climate archives and proxies such as hyrax dung and optically stimulated luminescence dating have led to relatively more spatio-temporal coverage of paleoclimate information for southwest Africa (Chase et al., 2009, 2011; Chase and Thomas, 2006, 2007; Meadows et al., 2010; Meadows and Sugden, 1991; Scott and Woodborne, 2007a, b). These records, along with the most recent high-resolution climate reconstruction of the Late Holocene from the western coastal area of South Africa (Benito et al., 2011; Stager et al., 2012), reveal that the WRZ of South Africa was very sensitive to centennial- and millennial-scale climate oscillations during the Holocene epoch. Notwithstanding the increasing number of paleo-records, the regional significance of and temporal correlation between the local climate signals and their link to surface water conditions of the adjacent ocean remain uncertain. Our study adds to the emerging pattern of past climate variability in southwest Africa by providing a spatially integrated record of terrestrial climate changes and its link to adjacent coastal water conditions that allow us to infer possible climatic links to the Southern

CPD

9, 2309–2356, 2013

### Holocene climate variability in the Winter Rainfall Zone of South Africa

S. Weldeab et al.

[Title Page](#)

[Abstract](#)

[Introduction](#)

[Conclusions](#)

[References](#)

[Tables](#)

[Figures](#)

[⏪](#)

[⏩](#)

[◀](#)

[▶](#)

[Back](#)

[Close](#)

[Full Screen / Esc](#)

[Printer-friendly Version](#)

[Interactive Discussion](#)



Hemisphere westerlies and the leakage of warm Agulhas water into the southeastern Atlantic.

## 2 Regional setting

The Winter Rainfall Zone (WRZ) of southwestern Africa stretches along the south-eastern Atlantic coastal region from southwestern Namibia to Cape Agulhas and extends inland to the western margin of the Great Escarpment (Chase and Meadows, 2007; MacKellar et al., 2007) (Fig. 1). The WRZ receives < 65 % of the annual rainfall during the austral winter, and consists of arid and semi-arid regions including the southern Namib Desert and the Namaqualand of South Africa (Chase and Meadows, 2007; MacKellar et al., 2007; Cowling et al., 1999). Along the coastal area, precipitation varies between 50 mm and 350 mm per year with marked local patterns (MacKellar et al., 2007).

The Namaqualand borders on dynamic coastal waters that are marked by inner-shelf upwellings that prevail throughout the year with enhanced intensity during the austral winter (Hardman-Mountford et al., 2003). This upwelling area constitutes the southern BUS whose intensity is driven by the strength and position of the southeasterly trade winds (Hardman-Mountford et al., 2003). On average, sea surface temperature and salinity account for 13.5 °C and 35 practical salinity unit (psu) during the austral winter and 16.9 °C and 34.9 psu during the austral summer (Locarnini et al., 2010). Within the southern BUS, localized cells of strong upwelling exist, including the Namaqua cell (Hardman-Mountford et al., 2003) from which the GeoB8332-4 was recovered. On interannual and interdecadal time scales, a weakening of the southern BUS occurs in response to a southward shift of the austral westerlies that allows the intrusion of warm Agulhas surface water into the southeastern Atlantic (Hardman-Mountford et al., 2003; Biastoch et al., 2009).

We focus on a marine sediment sequence recovered from the mudbelt whose detrital composition is determined by fluvial and eolian sediment inputs from the Orange

CPD

9, 2309–2356, 2013

### Holocene climate variability in the Winter Rainfall Zone of South Africa

S. Weldeab et al.

[Title Page](#)

[Abstract](#)

[Introduction](#)

[Conclusions](#)

[References](#)

[Tables](#)

[Figures](#)

[⏪](#)

[⏩](#)

[◀](#)

[▶](#)

[Back](#)

[Close](#)

[Full Screen / Esc](#)

[Printer-friendly Version](#)

[Interactive Discussion](#)



River, the Namaqualand, and the Namib Desert. The mudbelt is a prominent Holocene sediment package that covers a narrow strip along the inner-shelf between the Kunene River in the northwest and St. Helena Bay in the southeast (Compton et al., 2009, 2010; Herbert and Compton, 2007; Meadows et al., 2002; Rogers and Rau, 2006).

5 The Orange River presents the most dominant sediment source for the mudbelt with catchment area of 973 000 km<sup>2</sup>, runoff of 11 km<sup>3</sup> yr<sup>-1</sup>, and 60 million metric tons yr<sup>-1</sup> delivery of sediment (Bremner et al., 1990). Most of the Orange River runoff and suspended sediment comes from the easternmost catchment that receives an annual rainfall between 500 mm and > 750 mm during austral summer (Compton et al., 2010) (Fig. 1). Detailed mineralogical, chemical, and isotopic evidence indicates that the suspended sediments of Orange River mainly originate from the upper part of Ka-  
10 roo Supergroup (Late Triassic continental sedimentary rocks) (Compton and Maake, 2007; de Villiers et al., 2000). The Drakensberg Plateau, which is composed of flood basalt intersected by dolerite dykes/sills, receives high precipitation (> 750 mm yr<sup>-1</sup>), but contributes relatively small amounts to the total sediment load of the Orange River (Compton and Maake, 2007; de Villiers et al., 2000). Once it enters the Atlantic Ocean, waves and undercurrent distribute the massive sediment load of the Orange River. The sand fraction is swept northward by wave-driven littoral drifts (Meadows et al., 2002; Rogers and Rau, 2006). Northwesterly undercurrents distribute clayey-silty material to  
15 the southeast of the Orange River mouth, with decreasing grain size toward the south-eastern end of the mudbelt (Meadows et al., 2002; Rogers and Rau, 2006).

Ephemeral (Holgat and Buffels) and perennial (Olifants and Berg) rivers drain the western coastal area of South Africa (Fig. 1) that consists of Precambrian sedimentary rocks (> 2.5 billion years (Ga) old) and intrusions of 1 Ga granite and gneiss (Cowling et al., 1999). With a total catchment area of ~65 200 km<sup>2</sup> and an arid/semi-arid climate, the overall sediment contribution of the local rivers to the mudbelt is estimated to be relatively small (a quantitative estimate is not available) as compared to that of the Orange River (Herbert and Compton, 2007; Meadows et al., 2002; Rogers and  
25 Rau, 2006). Notable sedimentary imprint of the ephemeral rivers is found in sediment

CPD

9, 2309–2356, 2013

## Holocene climate variability in the Winter Rainfall Zone of South Africa

S. Weldeab et al.

Title Page

Abstract

Introduction

Conclusions

References

Tables

Figures

⏪

⏩

◀

▶

Back

Close

Full Screen / Esc

Printer-friendly Version

Interactive Discussion





## Holocene climate variability in the Winter Rainfall Zone of South Africa

S. Weldeab et al.

[Title Page](#)

[Abstract](#)

[Introduction](#)

[Conclusions](#)

[References](#)

[Tables](#)

[Figures](#)

[⏪](#)

[⏩](#)

[◀](#)

[▶](#)

[Back](#)

[Close](#)

[Full Screen / Esc](#)

[Printer-friendly Version](#)

[Interactive Discussion](#)

in 100 mL deionized water were added to the sediment and the mixture was boiled for 10 min. The solution was diluted with deionized water to neutral pH. Prior to grain-size analysis, the remaining terrigenous fraction was boiled with 300 mg of soluble sodium pyrophosphate ( $\text{Na}_4\text{P}_2\text{O}_7 \cdot 10\text{H}_2\text{O}$ ) to foster particle disaggregation. Grain-size analysis was performed using a Coulter laser particle sizer LS200. The analysis resulted in 92 size classes varying from 0.39 to 2000  $\mu\text{m}$ . An end-member modeling algorithm was applied to determine the proportions of distinct sediment components contributing to the measured particle size signal (Weltje, 1997; Stuut et al., 2002) (Fig. 3a–e). The algorithm output is a series of models, each containing a different number of “end-members”, and each model explaining a different amount of variance. The higher the number of end-members the more variance is explained (Fig. 3d). Two key parameters are used to determine the minimum number of end-members required for a satisfactory approximation of the measured data (Prins et al., 2000; Stuut et al., 2002; Weltje, 1997). First, the coefficient of determination per size class ( $r^2$ ) is used to assess how well the model reproduces the data in each size class (Fig. 3c). Second, the mean coefficient of determination ( $r_{\text{mean}}^2$ ) averaged for all size classes is used to test how well each model reproduces the average of all measured size classes (Fig. 3d). In this study, the model with a minimum number of 3 end-members (EM1, EM2, and EM3), with  $r^2 > 0.5$  and  $r_{\text{mean}}^2$  equal to 0.79 represents the best compromise (Fig. 3).

Time series of major element intensities were generated at 1 cm sampling interval using the Aavatech XRF Scanner I at the University of Bremen. The Core Scanner was run with an excitation potential of 10 kV, a current of 250  $\mu\text{A}$ , and 30 s counting time. Element intensities were normalized by dividing the total counts for each element by the sum of total counts for all measured elements. In this study we focus only on Ca/Al, K/Al and Ti/Al ratios (Fig. 4).

We analysed  $\delta^{18}\text{O}$  and  $\delta^{13}\text{C}$  in tests of *Neogloboquadrina pachyderma* (sinistral) (125–300  $\mu\text{m}$ ) from down core samples using a Thermo MAT 253 mass spectrometer at the first author’s stable isotope lab at UCSB. The mass spectrometer is coupled online to a Kiel IV Carbonate Device for automated  $\text{CO}_2$  preparation. Samples were

reacted by automated individual phosphoric acid addition. Results were corrected using NBS19 standard and are reported on the Pee Dee Belemnite (PDB) scale. Estimates for standard error ( $2\sigma$ ) in the  $\delta^{18}\text{O}$  and  $\delta^{13}\text{C}$  measurements are better than  $\pm 0.07\%$  and  $\pm 0.03\%$ , respectively.

Analyses of the  $^{87}\text{Sr}/^{86}\text{Sr}$  and  $^{143}\text{Nd}/^{144}\text{Nd}$  ratios on the lithogenic fraction ( $\leq 120\ \mu\text{m}$ ) of marine and riverine sediments were conducted on a Finnigan MAT 262 mass spectrometer using static collection mode at the Institute of Geosciences, University of Tübingen. In order to remove the carbonate fractions of down core samples, 500 mg of sediment was leached with 10 mL acetic acid (5 M) at room temperature for 12 h. The detrital residues were rinsed four times with ultrapure water, centrifuged, and the supernatant was removed. A 50-mg portion of the powdered and homogenized lithogenic fraction was spiked with a mixed  $^{149}\text{Sm}:^{150}\text{Nd}$  spike prior to digestion in HF. The digested samples were dried and dissolved in 6 N HCl, dried and then redissolved in 2.5 N HCl. Analyses of NBS-SRM 987 and La Jolla Nd standards during this study yielded an average value of  $^{87}\text{Sr}/^{86}\text{Sr} = 0.710244 \pm 15$  and for  $^{143}\text{Nd}/^{144}\text{Nd} = 0.511823 \pm 15$ , respectively.  $^{87}\text{Sr}/^{86}\text{Sr}$  ratios are normalized to  $^{86}\text{Sr}/^{88}\text{Sr} = 0.1194$  and the  $^{143}\text{Nd}/^{144}\text{Nd}$  ratios to  $^{146}\text{Nd}/^{144}\text{Nd} = 0.7219$ . Results of Nd and Sr in blank measurements are 80 pg and 65 pg, respectively. The  $^{143}\text{Nd}/^{144}\text{Nd}$  ratios are expressed as  $\epsilon\text{Nd}$ , where  $\epsilon\text{Nd}$  is the analyzed  $^{143}\text{Nd}/^{144}\text{Nd}$  ratio normalized to the “chondritic uniform reservoir” value (0.512638, (Jacobson and Wasserburg, 1980).

## 4 Results

### 4.1 Variations of terrigenous particle size

The particle size frequency distribution shows a bi-modal distribution pattern (Fig. 3a). The time series of the median grain size is marked by a continuous increase of particle size from the early to middle Holocene and declining trends between 5500 and 5000 yr BP as well as over the last 700 yr (Fig. 3b). We used an end-member modeling

CPD

9, 2309–2356, 2013

## Holocene climate variability in the Winter Rainfall Zone of South Africa

S. Weldeab et al.

Title Page

Abstract

Introduction

Conclusions

References

Tables

Figures

⏪

⏩

◀

▶

Back

Close

Full Screen / Esc

Printer-friendly Version

Interactive Discussion



## Holocene climate variability in the Winter Rainfall Zone of South Africa

S. Weldeab et al.

[Title Page](#)

[Abstract](#)

[Introduction](#)

[Conclusions](#)

[References](#)

[Tables](#)

[Figures](#)

[⏪](#)

[⏩](#)

[◀](#)

[▶](#)

[Back](#)

[Close](#)

[Full Screen / Esc](#)

[Printer-friendly Version](#)

[Interactive Discussion](#)

is too weak to carry sand and coarse silt fractions, it transports the fine silt and clay components of the Orange sediment load to the southeastern segment of the mudbelt (Mabote, 1997; Rogers and Rau, 2006). Our core site is located 57 km away from the delta of the Orange River (Fig. 1), and the median grain size of the core top samples (100–200 yr BP) shows value of 4  $\mu\text{m}$ , a sedimentation rate of 2 mm per year, and EM3 and EM2 explaining more than 97 % of the grain size variation. This observation shows that only the fine fraction ( $\leq 10 \mu\text{m}$ ) of Orange River sediment arrive at our core site. Based on the dominance of the fine fraction, we hypothesize that EM3 presents a fluvial component, an assumption that is supported by the element ratios and isotope signatures shown below.

Dust input from the Namib Desert and the Namaqualand presents an important sediment source for the southeastern Atlantic and the mudbelt (Mabote, 1997; Shannon and Anderson, 1982; Stuut et al., 2002; Mahowald et al., 2005). A model based study estimates that dust deposition off the Holgat River accounts for 7–10  $\text{g m}^{-2} \text{yr}^{-1}$  (Mahowald et al., 2005) for which no grain size analysis is available. Analysis of grain size of dust collected above the Walvis Ridge (Stuut et al., 2002) shows a broad uni-modal distribution with a modal value of 20  $\mu\text{m}$  that is very similar to that of EM1 (Fig. 3e). Due to the proximity of the dust source to our core site, it is most likely that an enhanced dust deposition leads to an increase of grain size. In our time series, EM1 presents the end-member with the largest model grain size of 20  $\mu\text{m}$ . EM1 and EM2 increased significantly during the mid Holocene. Based on the proximity of the dust sources to our core site and the weak bottom water current, we hypothesize that EM1 reflects sediment largely related to dust input. Following the approach described by Stuut et al. (2002, 2004), we calculated indices for relative humidity ( $\text{EM3}/(\text{EM1} + \text{EM2} + \text{EM3})$ ) and wind strength changes ( $\text{EM1}/(\text{EM1} + \text{EM2})$ ) throughout investigated time interval (see discussion section).

Exploring whether a strengthening of northeasterly bottom water current or an increase of sediment input from local rivers could have contributed to the mid Holocene

increase of grain size, it requires additional insights from the radiogenic and element record that is described below.

## 4.2 Variation of selected major elements

Figure 4 shows down core variation of Ca/Al, K/Al, and Ti/Al intensity ratios. Ca/Al primarily reflects changes in biogenic carbonate and shows that carbonate productivity was relatively high between 11 500 and 6750 yr BP, followed by a continuous decline. We focus on K/Al and Ti/Al to address changes in terrigenous input and to infer possible weathering and transport mechanisms. On millennial scale, K/Al ratios show a continuous decline starting from 11 500 to 6000 yr BP. An increasing K/Al trend is evident between 5500 and 5000 yr BP and during the last 700 yr BP. A millennial-scale trend in Ti/Al reveals increasing values from the early to middle Holocene and declining values from 6500 to 5000 yr BP as well as from 700 to 100 yr BP. Overall, millennial-scale trends in K/Al and Ti/Al ratios evolve in divergent directions, indicating different sources, weathering, or transport mechanisms. Clay mineralogical and chemical analyses of soil and suspended sediments in the catchment of the Orange River reveal that erosion products of the Karoo Supergroup series (Tertiary sedimentary rocks) are rich in illite, K-feldspar, smectite and show high K concentration (Compton and Maake, 2007). Furthermore, erosion products of the Karoo Supergroup series present the dominant fraction in the suspended sediment of the Orange River (Compton and Maake, 2007). Within the mudbelt between the Orange and the Olifants Rivers, concentration of K shows an increasing trend with low K values in the north (relatively proximal to the Orange River) as compared to those in the south (Govin et al., 2012). This distribution pattern arises due to grain size sorting by bottom currents, with coarse sediments in the north and predominantly clayey sediments in the south (Rogers and Rau, 2006). We suggest that temporal K/Al variation within our site indicates changes in K-rich fine sediments and the amount of fluvial input. A comprehensive analysis of major elements in Atlantic surface sediments, as well as a compilation dust and riverine suspended sediment data, indicate that with few exceptions high Ti/Al is related to enhanced dust

### Holocene climate variability in the Winter Rainfall Zone of South Africa

S. Weldeab et al.

[Title Page](#)

[Abstract](#)

[Introduction](#)

[Conclusions](#)

[References](#)

[Tables](#)

[Figures](#)

[⏪](#)

[⏩](#)

[◀](#)

[▶](#)

[Back](#)

[Close](#)

[Full Screen / Esc](#)

[Printer-friendly Version](#)

[Interactive Discussion](#)





## Holocene climate variability in the Winter Rainfall Zone of South Africa

S. Weldeab et al.

[Title Page](#)

[Abstract](#)

[Introduction](#)

[Conclusions](#)

[References](#)

[Tables](#)

[Figures](#)

[⏪](#)

[⏩](#)

[◀](#)

[▶](#)

[Back](#)

[Close](#)

[Full Screen / Esc](#)

[Printer-friendly Version](#)

[Interactive Discussion](#)

the water of the Vaal River (a major tributary of the Orange River) show, on average, a  $^{87}\text{Sr}/^{86}\text{Sr}$  ratio of 0.731 (de Villiers et al., 2000). This observation shows that more work is needed to decipher which minerals present the main source for dissolved Sr and which isotope values characterize suspended sediment loads in the main tributaries of the Orange River. Nonetheless, we argue that  $^{87}\text{Sr}/^{86}\text{Sr}$  signatures of  $\sim 0.73$  for suspended sediments in the Lower Orange River together with an  $\varepsilon\text{Nd}$  signature of  $-9.19 \pm 1.45$  ( $n = 3$ ) from Beaufort Group shales which form the upper portion of the Karoo Supergroup (Dia et al., 1990) may represent integrated isotope signatures for suspended sediments of the Orange River (Fig. 5). Average values of  $0.75318 \pm 0.02$  ( $n = 4$ ) and  $-16.9 \pm 2.05$  ( $n = 4$ ) for  $^{87}\text{Sr}/^{86}\text{Sr}$  and  $\varepsilon\text{Nd}$  signatures characterize riverbed sediments from the local rivers (Figs. 1 and 5, Table 2). We exclude the  $^{87}\text{Sr}/^{86}\text{Sr}$  and  $\varepsilon\text{Nd}$  values of Olifants River (Fig. 1 and Table 2) because we suspect that the sampling site is influenced by tide-mobilized sediments from the shallow water. A third sediment source is dust input from the Namib Desert. Analysis of Namib Desert dust samples (Grousset et al., 1992) shows average  $^{87}\text{Sr}/^{86}\text{Sr}$  and  $\varepsilon\text{Nd}$  value of  $0.72232 \pm 0.003$  ( $n = 8$ ) and  $-8.64 \pm 3.24$ , ( $n = 8$ ), respectively

$^{87}\text{Sr}/^{86}\text{Sr}$  and  $\varepsilon\text{Nd}$  values in the time series of the sediment core vary between 0.73493 and 0.719441 and  $-10.39$  and  $-11.74$ , respectively. The down-core variation of Nd isotope values is relatively small due to the dominance of Orange River sediments (Figs. 4 and 5). It is also important to note that changes in grain size have an effect on the  $^{87}\text{Sr}/^{86}\text{Sr}$  signature (Eisenhauer et al., 1999; Meyer et al., 2011). Because the down core record reveals significant grain size variation (Fig. 3b), the time series of  $^{87}\text{Sr}/^{86}\text{Sr}$  likely harbors an imprint of grain size changes. Therefore we emphasize that the assessment of changes in source or transport mechanism is best achieved by combining the results of all proxy parameters. Consistent with the time series of median grain size and K/Al (Figs. 3b and 4f), the radiogenic isotope signatures show a trend that is marked by decreasing  $^{87}\text{Sr}/^{86}\text{Sr}$  ratios and  $\varepsilon\text{Nd}$  values during the early Holocene (11 600 to 9000 yr BP). During the middle Holocene,  $^{87}\text{Sr}/^{86}\text{Sr}$  ratios continue to decrease until 6000 yr BP while  $\varepsilon\text{Nd}$  remains at a constant level similar to the end

of the Early Holocene (9000 yr BP). In contrast, the youngest time interval (700–0 BP) reveals increasing  $^{87}\text{Sr}/^{86}\text{Sr}$  ratios and decreasing  $\epsilon\text{Nd}$  values parallel to an increase in fluvial sediment supply, as suggested by the decrease in median grain-size, increase of EM3 and K/Al ratio (Fig. 3).

On the basis of the temporal patterns depicted in Figs. 4c–d and 5, the following relationship emerges between down-core variability of Sr and Nd isotopes and possible shifts in main sediment sources: from the early to middle Holocene,  $^{87}\text{Sr}/^{86}\text{Sr}$  and  $\epsilon\text{Nd}$  values decline from  $0.7336 \pm 0.0018$  ( $n = 2$ ) to  $0.7242 \pm 0.0042$  ( $n = 9$ ) and from  $-10.88 \pm 0.11$  ( $n = 2$ ) to  $-11.44 \pm 0.16$  ( $n = 9$ ), respectively. Concomitant increase in median grain size in the terrigenous sediments may have contributed to the relatively large decline in the  $^{87}\text{Sr}/^{86}\text{Sr}$  ratio. High Ti/Al values and the dominance of EM1 with a modal grain size of  $\sim 20 \mu\text{m}$  correspond with the changes in the Sr and Nd isotopes. This suggests an enhanced influence of eolian input or coarse fluvial sediment input from the Holgat River during the middle Holocene. However, the relatively low sedimentation rate and low K/Al ratio argue against increased fluvial influence. From 700 yr BP toward the core top,  $^{87}\text{Sr}/^{86}\text{Sr}$  and  $\epsilon\text{Nd}$  reveal increasing and declining values, respectively. This trend is accompanied by changes in median grain size from coarse to fine silt and clay, an increase in the K/Al, and a decrease in Ti/Al. Changes in all parameters thus indicate increase of river sediment supply over the last 700 yr. More important, the negative trend in  $\epsilon\text{Nd}$  and an increase in  $^{87}\text{Sr}/^{86}\text{Sr}$  suggest a relative increase of sediment input from the local rivers.

#### 4.4 $\delta^{18}\text{O}$ and $\delta^{13}\text{C}$ in tests of *Neogloboquadrina pachyderma* (sinistral)

The results of  $\delta^{18}\text{O}$  and  $\delta^{13}\text{C}$  analysis in tests of *Neogloboquadrina pachyderma* (sinistral) are shown in Fig. 4a and b. The long-term carbon isotope trend is marked by an increase of  $\delta^{13}\text{C}$  from an average value of  $-1.1 \pm 0.17$  ( $n = 55$ ) between 10 800 and 7000 yr BP to  $-0.54 \pm 0.19$  ( $n = 21$ ) between 6800 and 5100 yr BP. On average, a decreasing trend in  $\delta^{13}\text{C}$  is evident in the youngest section of the record (100–700 yr BP), showing a mean value of  $-0.18 \pm 0.1$  ( $n = 26$ ).

## Holocene climate variability in the Winter Rainfall Zone of South Africa

S. Weldeab et al.

Title Page

Abstract

Introduction

Conclusions

References

Tables

Figures

⏪

⏩

◀

▶

Back

Close

Full Screen / Esc

Printer-friendly Version

Interactive Discussion



## Holocene climate variability in the Winter Rainfall Zone of South Africa

S. Weldeab et al.

[Title Page](#)

[Abstract](#)

[Introduction](#)

[Conclusions](#)

[References](#)

[Tables](#)

[Figures](#)

[⏪](#)

[⏩](#)

[◀](#)

[▶](#)

[Back](#)

[Close](#)

[Full Screen / Esc](#)

[Printer-friendly Version](#)

[Interactive Discussion](#)



Changes in the isotope signature of dissolved inorganic carbon (DIC) and its manifestation in the carbon isotope composition of planktonic foraminiferal tests can be influenced by several processes. Due to the hydrographic, bathymetric, and depositional setting of our core site, a relatively low organic matter burial efficiency coupled with suspension and vertical mixing by bottom currents and internal waves (Compton et al., 2009), and ensuing demineralization of organic matter may present a source of DIC variability. Estimates of particulate and dissolved organic matter from the Orange River entering the delta system, on average, account for  $62\,000\text{ ton yr}^{-1}$ , and approximately half of this amount is buried in the subaqueous delta plains (Compton et al., 2009).  $\delta^{13}\text{C}$  values of organic matter in soil and suspended matter in the catchment and tributaries of the Orange River cover a wide range, varying between  $-12.7$  and  $-21.5\text{‰}$  (Compton and Maake, 2007). In contrast, measurements of  $\delta^{13}\text{C}$  in organic matter along the mudbelt show rapidly decreasing  $\delta^{13}\text{C}$  values away from riverine influenced zone, suggesting that most of the riverine organic matter is composed of  $\text{C}_4$  plant remains and that it is deposited predominantly in the delta and prodelta systems (Meadows et al., 2002). Approximately 42 km southeast of the Orange River mouth, the average value of  $\delta^{13}\text{C}$  in organic matter is  $\sim -19.8\text{‰}$ , which is close to the average value of marine organic matter (varying between  $-20$  and  $-21\text{‰}$ ) (Meadows et al., 2002). Our core site is approximately 57 km southeast of the Orange River delta. Therefore, the influence of riverine DIC over our site is low, and wind-induced upwelling of demineralized marine organic carbon provides the dominant source of DIC. Hence, the long-term variability of  $\delta^{13}\text{C}$  in our record may indicate changes in the strength of coastal water upwelling, with relatively low  $\delta^{13}\text{C}$  values indicating strong upwelling.

The  $\delta^{18}\text{O}$  record reflects a composite imprint of changes in continental ice volume, calcification temperature, and fresh water input. We removed the ice volume component from the foraminiferal  $\delta^{18}\text{O}$  record using the eustatic level record from Bard et al. (1996). A prominent feature in the ice volume corrected  $\delta^{18}\text{O}$  ( $\delta^{18}\text{O}_{\text{IVC}}$ ) record throughout the early and middle Holocene is a gradually declining trend that is interrupted by precipitous rises in  $\delta^{18}\text{O}_{\text{IVC}}$ . On multi-centennial to millennial scale,



## Holocene climate variability in the Winter Rainfall Zone of South Africa

S. Weldeab et al.

[Title Page](#)

[Abstract](#)

[Introduction](#)

[Conclusions](#)

[References](#)

[Tables](#)

[Figures](#)

[⏪](#)

[⏩](#)

[◀](#)

[▶](#)

[Back](#)

[Close](#)

[Full Screen / Esc](#)

[Printer-friendly Version](#)

[Interactive Discussion](#)

signature is small. In order to assess the link between changes in the amount of sediment with Orange River eNd signature and climate conditions in the Orange River catchment, we compare our record with those from eastern South Africa where the main tributaries of the Orange River originate. Re-evaluations of several pollen records within the Orange River catchment and northeast of the catchment (Scott et al., 2008, 2012) suggest a heterogeneous pattern between these closely located sites. The Braamhoek pollen record (within the Orange River catchment) suggests relatively wet conditions through the early Holocene with slight drying trend toward the mid Holocene (Scott et al., 2012). A pollen record from the northeastern periphery of the Orange River basin (Rietvlei swamp) largely supports the climate trend as suggested by the Braamhoek pollen record (Scott et al., 2012). Farther northeast from the Orange basin, the early and mid Holocene climate trend, as suggested by the Wonderkrater pollen record (Scott et al., 2012) and biomarker record from Tswaing Crater (Kristen et al., 2010), is markedly different from that of Braamhoek and Rietvlei records (Scott et al., 2012). The Wonderkrater (Scott et al., 2012) and Tswaing records (Kristen et al., 2010) suggest early Holocene (11 500–10 000 yr BP) humid conditions that gave way to mid Holocene (9500–6500 yr BP) dry conditions (Fig. 6j and k). The comparison indicates that a link exists between humid climate conditions in eastern South Africa and an increase of fine components (EM3 and EM2) in the terrigenous sediment of Geo8332-4. Between 9500 and 7500 yr BP, the decrease of moisture in eastern South Africa (Fig. 6j and k) parallels the decline of EM3. The onset of humid climate conditions around 7500–7000 yr BP in eastern South Africa corresponds with increase of EM1, indicating relatively dry conditions in the coastal area.

The highest value of EM1, the end-member with the largest modal grain size of 20  $\mu\text{m}$ , and more negative eNd value indicating a relatively enhanced eolian contribution from the Namaqualand occurred at time (7500–5000 yr BP) when humid climate conditions were established in eastern South Africa (Fig. 4d). Increase in dust input, most likely due to strengthened or more frequent easterly winds, was accompanied by a continuous weakening of coastal upwelling and surface water warming, as suggested







## Holocene climate variability in the Winter Rainfall Zone of South Africa

S. Weldeab et al.

[Title Page](#)

[Abstract](#)

[Introduction](#)

[Conclusions](#)

[References](#)

[Tables](#)

[Figures](#)

[⏪](#)

[⏩](#)

[◀](#)

[▶](#)

[Back](#)

[Close](#)

[Full Screen / Esc](#)

[Printer-friendly Version](#)

[Interactive Discussion](#)

Indian Ocean sectors (Beal et al., 2011). Instrumental and modeling studies demonstrate that southward displacement of the austral westerlies and attendant southward shift of the subtropical front enable an increased leakage of warm and saline Agulhas water into the southern Atlantic (Beal et al., 2011; Biastoch et al., 2008, 2009; Shannon et al., 1990). Modern observations also show that the incursion of Agulhas water into the southern BUS warms the surface water and weakens the coastal upwelling due changes in the density structure of surface water (Hardman-Mountford et al., 2003; Biastoch et al., 2009; Lutjeharms et al., 2001). Rainfall observations in the WRZ between 1950 and 1999 show that with exception of the central area winter rainfall declined significantly in the southern, northern, and inland of the WRZ of Namaqualand (MacKellar et al., 2007). Overall, instrumental observations of the last 4–5 decades of the last century show that there is a clear temporal coincidence and most likely causal links between southward displacement of austral westerlies and subtropical front, enhanced Agulhas leakage, increase in  $nss-Ca^{2+}$  accumulation over Antarctica, a weakening of the southern BUS, and decline of winter rainfall in large part of the Namaqualand. Therefore based on the links deduced from modern observations we suggest that the middle Holocene dry conditions in the Namaqualand and the weakening of the southern BUS most likely were linked to a poleward shift of the austral westerlies and an enhanced amount of Agulhas water leakage, as indicated by geochemical analysis in Antarctic ice core (Roethlisberger et al., 2002) and shift in planktonic foraminiferal composition off South Africa (Peeters et al., 2004), respectively (Fig. 6a and b). Furthermore, we suggest that increased leakage of Agulhas water into the southern BUS and resultant warming of the coastal water during the middle Holocene may have reduced coastal fog formation. At present, coastal fog formation over the cold upwelled coastal water presents an important moisture source for the flora of Namaqualand (Cowling et al., 1999; MacKellar et al., 2007). Warming of the coastal water reduces the thermal gradient between air and surface water temperature and fog formation.

Stager et al. (2012) suggest that increase in  $nss-Ca^{2+}$  concentration in the Siple Dome ice core (western Antarctica) may be related to equatorward shift of the austral



(Herbert and Compton, 2007 and references therein) as well as pulses of freshening events evident in the Lake Verlorenvlei record (Stager et al., 2012) (Figs. 1 and 7k) over the last 700–600 yr lend credence to our Nd and Sr isotope-based inference of increased sediment contribution from the local rivers.

The increase in fluvial sediments of proximal origin between 600 and 100 yr BP falls within the time interval of global climate instability known as the “Little Ice Age” (LIA). In the Northern Hemisphere, the duration of the LIA encompasses the time between 1300 and 1850 Common Era (CE) (Holzhauser et al., 2005; Miller et al., 2012). Elsewhere, the timing of the northern cold spell is less well constrained, owing to dating uncertainties and interhemispheric difference in the onset and termination of this climatic event (Schaefer et al., 2009). While anthropogenic contribution to the enhanced sediment mobilization at least during the younger part of the time series cannot be ruled out, we argue that our record largely reflects a regional expression of the global climate event associated with the LIA. Our data suggest that the winter rainfall zone of South Africa experienced humid conditions over the last 600 yr. Considering age model uncertainties that can account up to  $\pm 100$  yr, the onset of humid phase in the WRZ of southwestern Africa at  $600 \pm 50$  yr BP is coincident with these of glacier advances in New Zealand at  $\sim 570$  yr (Schaefer et al., 2009), lake level high stand at  $\sim 500$  BP in Patagonia (Stine and Stine, 1990), dominance of wet climate-indicating pollen record from southern South America (Moreno et al., 2010), increased precipitation in southwestern Patagonia at around 575 yr BP (Moy et al., 2008), and the onset of decrease in  $nss\text{-Ca}^{2+}$  accumulation of in Antarctica ice cores at  $\sim 650$  yr BP (Fig. 7a). With the exception of multi-decadal increase between 200 and 150 yr BP,  $nss\text{-Ca}^{2+}$  concentration remained low between 650 and 100 yr BP. Therefore, the increase in precipitation within the WRZ was linked to a large-scale atmospheric reorganization in mid-latitudes of the Southern Hemisphere. The early onset of the relatively humid conditions in the WRZ is contrasted by high Ti/Al and coarse grain sizes (EM1) (Fig. 7f and g). This probably indicates that dust input remained relatively high until approximately 400 yr BP. We note that the dust source extends deep into the northern and western summer

## Holocene climate variability in the Winter Rainfall Zone of South Africa

S. Weldeab et al.

[Title Page](#)

[Abstract](#)

[Introduction](#)

[Conclusions](#)

[References](#)

[Tables](#)

[Figures](#)

[⏪](#)

[⏩](#)

[◀](#)

[▶](#)

[Back](#)

[Close](#)

[Full Screen / Esc](#)

[Printer-friendly Version](#)

[Interactive Discussion](#)







## Holocene climate variability in the Winter Rainfall Zone of South Africa

S. Weldeab et al.

[Title Page](#)

[Abstract](#)

[Introduction](#)

[Conclusions](#)

[References](#)

[Tables](#)

[Figures](#)

[⏪](#)

[⏩](#)

[◀](#)

[▶](#)

[Back](#)

[Close](#)

[Full Screen / Esc](#)

[Printer-friendly Version](#)

[Interactive Discussion](#)

intensification or more frequent incursion of easterly winds known as Berg winds. The coincidence of local wind intensification and dune formation along the coastal area of northwestern South Africa (Chase and Thomas, 2006) may suggest a more prominent role of the northeasterly and easterly wind strength in the formation of the dunes.

Corroborating recent findings in sediment sequences of the Buffels River (Benito et al., 2011) and Lake Verlorenvlei (Stager et al., 2012), our study indicates that the coastal area of southwestern Africa experienced increasingly wet climate conditions during the last 600 yr BP. Furthermore, the multi-proxy record provides key hints as how the SRZ have climatically evolved during the LIA. The onset of relatively humid conditions in the SRZ lags by  $\sim 200$  yr relative to that of the WRZ. The delayed onset corresponds to the timing of a significant weakening of heat export to the North Atlantic from the tropics (Lund and Curry, 2006) and a large-scale southward displacement of the ITCZ towards South Africa (Johnson et al., 2001; Haug et al., 2001). Hence, while a northward expansion of the humid WRZ into the arid SRZ cannot be ruled out, a southward shift of the ITCZ may have played a more dominant role in bringing more moisture to the SRZ.

The relatively wet phase in the WRZ during the Northern Hemisphere LIA shares many features in common with climate records of mid-latitude South America and New Zealand, most likely indicating a common cause. Climate models point to the critical role that a latitudinal shift of westerlies could have played in modulating past precipitation in the subtropical and mid-latitudes (Cockcroft et al., 1987; Toggweiler et al., 2006; Tyson et al., 2002). Our study provides evidence that the wet episodes in the coastal area of southwestern Africa were accompanied by relatively strong upwelling and cold surface waters. Conversely, the middle Holocene gradual aridification trend was paralleled by a weakening of the southern BUS. These observations are consistent with a latitudinal shift of austral mid-latitude westerlies and varying amount of Agulhas water leakage into the southern BUS.

The findings of this study highlight the linkage between terrestrial climate in the coastal area and the variability of the southern BUS, and gives us a better

## Holocene climate variability in the Winter Rainfall Zone of South Africa

S. Weldeab et al.

[Title Page](#)

[Abstract](#)

[Introduction](#)

[Conclusions](#)

[References](#)

[Tables](#)

[Figures](#)

[⏪](#)

[⏩](#)

[◀](#)

[▶](#)

[Back](#)

[Close](#)

[Full Screen / Esc](#)

[Printer-friendly Version](#)

[Interactive Discussion](#)

understanding of the southwestern Africa climate regime and its link to mid-latitude atmospheric and ocean circulation. Based on the temporal and most likely causal relationship between the middle Holocene dry climate conditions in the WRZ, weakening of the southern BUS, increased leakage of warm Agulhas water, and poleward shifts of the austral mid-latitude westerlies, our findings lend strong support to the notion that in the context of global climate change southward shifts of the westerlies may result in a weakening of precipitation in the WRZ, and a decline in upwelling intensity, with implications for phytoplankton productivity and local fisheries. Furthermore, increasing leakage of Agulhas water as result of southward shift of the westerlies may cause further warming of the surface water and reduction coastal fog formation.

*Acknowledgements.* We thank the Captain, Crew, and participants of *Meteor Cruise M53-6*. We thank John Compton (University of Cape Town, South Africa) for providing a sediment sample from Alexander Bay, Holly Avery for help with stable isotope sample preparation, Gerrit-Jan Weltje for providing the End-Member Modeling Algorithm software, and Dorothy Pak for comments. We thank Stager and an anonymous reviewer for their insightful and constructive comments. We also thank Claussen for his editorial handling of this paper. Weldeab is grateful to UCSB for a generous start-up package.

This is a resubmission of a manuscript that was handled by Dr. Martin Claussen.

## References

- Bard, E., Hamelin, B., Arnold, M., Montaggioni, L., Cabioch, G., Faure, G., and Rougerie, F.: Deglacial sea-level record from Tahiti corals and the timing of global meltwater discharge, *Nature*, 382, 241–244, 1996.
- Bayon, G., German, C. R., Nesbitt, R. W., Bertrand, P., and Schneider, R. R.: Increased input of circumpolar deep water-borne detritus to the glacial SE Atlantic Ocean, *Geochem. Geophys. Geosyst.*, 4, 1025, doi:10.1029/2002GC000371, 2003.
- Beal, L. M., De Ruijter, W. P. M., Biastoch, A., and Zahn, R.: On the role of the Agulhas system in ocean circulation and climate, *Nature*, 472, 429–436, 2011.

---

## Holocene climate variability in the Winter Rainfall Zone of South Africa

S. Weldeab et al.

---

[Title Page](#)

[Abstract](#)

[Introduction](#)

[Conclusions](#)

[References](#)

[Tables](#)

[Figures](#)

[⏪](#)

[⏩](#)

[◀](#)

[▶](#)

[Back](#)

[Close](#)

[Full Screen / Esc](#)

[Printer-friendly Version](#)

[Interactive Discussion](#)



Bemis, B. E., Spero, H., Bijma, J., and Lea, D. W.: Reevaluation of oxygen isotope composition of planktonic foraminifera: experimental results and revised paleotemperature equations, *Paleoceanography*, 13, 150–160, 1998.

Benito, G., Thorndycraft, V. R., Rico, M. T., Sanchez-Moya, Y., Sopena, A., Botero, B. A., Machado, M. J., Davis, M., and Perez-Gonzalez, A.: Hydrological response of a dryland ephemeral river to southern African climatic variability during the last millennium, *Quaternary Res.*, 75, 471–482, doi:10.1016/j.yqres.2011.01.004, 2011.

Biaostoch, A., Boning, C. W., and Lutjeharms, J. R. E.: Agulhas leakage dynamics affects decadal variability in Atlantic overturning circulation, *Nature*, 456, 489–492, doi:10.1038/nature07426, 2008.

Biaostoch, A., Boning, C. W., Schwarzkopf, F. U., and Lutjeharms, J. R. E.: Increase in Agulhas leakage due to poleward shift of Southern Hemisphere westerlies, *Nature*, 462, 495–498, doi:10.1038/nature08519, 2009.

Bremner, J. M., Rogers, J., and Willis, J. P.: Sedimentological aspects of the 1988 Orange River floods, *Transaction of the Royal Society of South Africa*, 47, 247–294, 1990.

Chase, B. M. and Thomas, D. S. G.: Late Quaternary dune accumulation along the western margin of South Africa: distinguishing forcing mechanisms through the analysis of migratory dune forms, *Earth Planet. Sci. Lett.*, 251, 318–333, doi:10.1016/j.epsl.2006.09.017, 2006.

Chase, B. M. and Meadows, M. E.: Late Quaternary dynamics of southern Africa's winter rainfall zone, *Earth-Sci. Rev.*, 84, 103–138, 2007.

Chase, B. M. and Thomas, D. S. G.: Multiphase late Quaternary aeolian sediment accumulation in western South Africa: Timing and relationship to palaeoclimatic changes inferred from the marine record, *Quaternary Int.*, 166, 29–41, 2007.

Chase, B. M., Meadows, M. E., Scott, L., Thomas, D. S. G., Marais, E., Sealy, J., and Reimer, P. J.: A record of rapid Holocene climate change preserved in hyrax middens from southwestern Africa, *Geology*, 37, 703–706, doi:10.1130/g30053a.1, 2009.

Chase, B. M., Meadows, M. E., Carr, A. S., and Reimer, P. J.: Evidence for progressive Holocene aridification in southern Africa recorded in Namibian hyrax middens: Implications for African Monsoon dynamics and the “African Humid Period”, *Quaternary Res.*, 74, 36–45, doi:10.1016/j.yqres.2010.04.006, 2010.

Chase, B. M., Quick, L. J., Meadows, M. E., Scott, L., Thomas, D. S. G., and Reimer, P. J.: Late glacial interhemispheric climate dynamics revealed in South African hyrax middens, *Geology*, 39, 19–22, doi:10.1130/g31129.1, 2011.

## Holocene climate variability in the Winter Rainfall Zone of South Africa

S. Weldeab et al.

[Title Page](#)

[Abstract](#)

[Introduction](#)

[Conclusions](#)

[References](#)

[Tables](#)

[Figures](#)

[⏪](#)

[⏩](#)

[◀](#)

[▶](#)

[Back](#)

[Close](#)

[Full Screen / Esc](#)

[Printer-friendly Version](#)

[Interactive Discussion](#)

Cockcroft, M. J., Wilkinson, M. J., and Tyson, P. D.: The application of a present-day climatic model to the late quaternary in southern Africa, *Climatic Change*, 10, 161–181, doi:10.1007/bf00140253, 1987.

Compton, J. S.: Holocene sea-level fluctuations inferred from the evolution of depositional environments of the southern Langebaan Lagoon salt marsh, South Africa, *The Holocene*, 11, 395–405, doi:10.1191/095968301678302832, 2001.

Compton, J. S. and Maake, L.: Source of the suspended load of the upper Orange River, South Africa, *S. Afr. J. Geol.*, 110, 339–348, doi:10.2113/gssajg.110.2-3.339, 2007.

Compton, J. S., Herbert, C., and Schneider, R.: Organic-rich mud on the western margin of southern Africa: Nutrient source to the Southern Ocean?, *Global Biogeochem. Cy.*, 23, Gb4030, doi:10.1029/2008gb003427, 2009.

Compton, J. S., Herbert, C. T., Hoffman, M. T., Schneider, R. R., and Stuut, J.-B.: A tenfold increase in the Orange River mean Holocene mud flux: implications for soil erosion in South Africa, *Holocene*, 20, 115–122, doi:10.1177/0959683609348860, 2010.

Cowling, R. M., Esler, K. J., and Rundel, P. W.: Namaqualand, South Africa: An Overview of a Unique Winter-Rainfall Desert Ecosystem, *Plant Ecol.*, 142, 3–21, 1999.

de Villiers, S., Compton, J. S., and Lavelle, M.: The strontium isotope systematics of the Orange River, Southern Africa, *S. Afr. J. Geol.*, 103, 237–248, doi:10.2113/1030237, 2000.

Dia, A., Allegre, C. J., and Erlank, A. J.: The development of continental crust through geological time: the South African case, *Earth Planet. Sci. Lett.*, 98, 74–89, 1990.

Dixon, D. A., Mayewski, P. A., Goodwin, I. D., Marshall, G. J., Freeman, R., Maasch, K. A., and Sneed, S. B.: An ice-core proxy for northerly air mass incursions into West Antarctica, *Int. J. Climatol.*, 32, 1455–1465, doi:10.1002/joc.2371, 2011.

Douglass, D. C., Singer, B. S., Kaplan, M. R., Ackert, R. P., Mickelson, D. M., and Caffee, M. W.: Evidence of early Holocene glacial advances in southern South America from cosmogenic surface-exposure dating, *Geology*, 33, 237–240, doi:10.1130/g21144.1, 2005.

Eisenhauer, A., Meyer, H., Rachold, V., Tuetken, T., Wiegand, B., Hansen, B. T., Spielhagen, R. F., Lindemann, F., and Kassens, H.: Grain size separation and sediment mixing in Arctic Ocean sediments: evidence from the strontium isotope systematic, *Chem. Geol.*, 158, 173–188, 1999.

Govin, A., Holzwarth, U., Heslop, D., Ford Keeling, L., Zabel, M., Mulitza, S., Collins, J. A., and Chiessi, C. M.: Distribution of major elements in Atlantic surface sediments

## Holocene climate variability in the Winter Rainfall Zone of South Africa

S. Weldeab et al.

[Title Page](#)

[Abstract](#)

[Introduction](#)

[Conclusions](#)

[References](#)

[Tables](#)

[Figures](#)

[⏪](#)

[⏩](#)

[◀](#)

[▶](#)

[Back](#)

[Close](#)

[Full Screen / Esc](#)

[Printer-friendly Version](#)

[Interactive Discussion](#)

- (368N&#8211;498S): Imprint of terrigenous input and continental weathering, *Geochem. Geophys. Geosyst.*, 13, Q01013, doi:10.1029/2011gc003785, 2012.
- Grousset, F. E. and Biscaye, P. E.: Tracing dust sources and transport patterns using Sr, Nd and Pb isotopes, *Chem. Geol.*, 222, 149–167, 2005.
- 5 Grousset, F., Biscaye, P. E., Revel, M., and Petit, J.-R.: Antarttic (Dome C) ice-core dust at 18 k.y. B.P.: Isotopic constraints on origins, *Earth Planet. Sci. Lett.*, 111, 175–182, 1992.
- Hardman-Mountford, N. J., Richardson, A. J., Agenbag, J. J., Hagen, E., Nykjaer, L., Shillington, F. A., and Villacastin, C.: Ocean climate of the South East Atlantic observed from satellite data and wind models, *Prog. Oceanogr.*, 59, 181–221, doi:10.1016/j.pocean.2003.10.001,
- 10 2003.
- Haug, G. H., Hughen, K. A., Sigman, D. M., Peterson, L. C., and Röhl, U.: Southward migration of the Intertropical Convergence Zone through the Holocene, *Science*, 293, 1304–1308, 2001.
- Heine, K.: Little Ice Age climatic fluctuations in the Namib Desert, Namibia, and adjacent areas: Evidence of exceptionally large floods from slack water deposits and desert soil sequences, in: *Paleocology of Quaternary Drylands*, edited by: Smykatz-Kloss, W. and Felix-Henningsen, P., *Lecture Notes in Earth Sciences*, Springer-Verlag, Springer Berlin/Heidelberg, 137–165, 2004.
- Herbert, C. T. and Compton, J. S.: Geochronology of Holocene sediments on the western margin of South Africa, *S. Afr. J. Geol.*, 110, 327–338, doi:10.2113/gssajg.110.2-3.327, 2007.
- 20 Holzhauser, H., Magny, M., and Zumbuhl, H. J.: Glacier and lake-level variations in west-central Europe over the last 3500 years, *Holocene*, 15, 789–801, doi:10.1191/0959683605hl853ra, 2005.
- Jacobson, S. B. and Wasserburg, G. J.: Sm-Nd isotopic evolution of chondrites, *Earth Planet. Sci. Lett.*, 50, 139–155, 1980.
- 25 Johnson, T. C., Barry, S. L., Chan, Y., and Wilkinson, P.: Decadal record of climate variability spanning the past 700 yr in the southern Tropics of East Africa, *Geology*, 29, 83–86, doi:10.1130/0091-7613(2001)029<0083:drocv>2.0.co;2, 2001.
- Lamy, F., Kaiser, J., Arz, H. W., Hebbeln, D., Ninnemann, U., Timm, O., Timmermann, A., and Toggweiler, J. R.: Modulation of the bipolar seesaw in the southeast pacific during Termination 1, *Earth Planet. Sci. Lett.*, 259, 400–413, doi:10.1016/j.epsl.2007.04.040, 2007.
- 30

## Holocene climate variability in the Winter Rainfall Zone of South Africa

S. Weldeab et al.

[Title Page](#)

[Abstract](#)

[Introduction](#)

[Conclusions](#)

[References](#)

[Tables](#)

[Figures](#)

[⏪](#)

[⏩](#)

[◀](#)

[▶](#)

[Back](#)

[Close](#)

[Full Screen / Esc](#)

[Printer-friendly Version](#)

[Interactive Discussion](#)



- Lamy, F., Kilian, R., Arz, H. W., Francois, J.-P., Kaiser, J., Prange, M., and Steinke, T.: Holocene changes in the position and intensity of the southern westerly wind belt, *Nat. Geosci.*, 3, 695–699, 2011.
- Leduc, G., Herbert, C. T., Blanz, T., Martinez, P., and Schneider, R.: Contrasting evolution of sea surface temperature in the Benguela upwelling system under natural and anthropogenic climate forcings, *Geophys. Res. Lett.*, 37, L20705, doi:10.1029/2010gl044353, 2010.
- Lund, D. C. and Curry, W.: Florida Current surface temperature and salinity variability during the last millennium, *Paleoceanography*, 21, PA2009, doi:10.1029/2005PA001218, 2006.
- Lutjeharms, J. R. E., Monteiro, P. M. S., Tyson, P. D., and Obura, D.: The oceans around southern Africa and regional effects of global change, *S. Afr. J. Sci.*, 97, 119–130, 2001.
- Mabote, M. E., Rogers, J., and Meadows, M. E.: Sedimentology of terrigenous mud from the orange river delta and the inner shelf off Namaqualand, South Africa, *S. Afr. Geogr. J.*, special edition, 108–114, 1997.
- MacKellar, N. C., Hewitson, B. C., and Tadross, M. A.: Namaqualand's climate: Recent historical changes and future scenarios, *J. Arid Environ.*, 70, 604–614, 2007.
- Mahowald, N. M., Baker, A. R., Bergametti, G., Brooks, N., Duce, R. A., Jickells, T. D., Kubilay, N. n., Prospero, J. M., and Tegen, I.: Atmospheric global dust cycle and iron inputs to the ocean, *Global Biogeochem. Cy.*, 19, GB4025, doi:10.1029/2004gb002402, 2005.
- Meadows, M. E. and Sugden, J. M.: A vegetation history of the last 14,000 years on the Cederberg, South-Western Cape Province, *S. Afr. J. Sci.*, 87, 34–43, 1991.
- Meadows, M. E., Rogers, J., Lee-Thorp, J. A., Bateman, M. D., and Dingle, R. V.: Holocene geochronology of a continental shelf mudbelt off southwestern Africa, *The Holocene*, 12, 59–67, doi:10.1191/0959683602h1521rp, 2002.
- Meadows, M. E., Chase, B. M., and Seliane, M.: Holocene palaeoenvironments of the Cederberg and Swaruggens mountains, Western Cape, South Africa: Pollen and stable isotope evidence from hyrax dung middens, *J. Arid Environ.*, 74, 786–793, doi:10.1016/j.jaridenv.2009.04.020, 2010.
- Meisel, S., Struck, U., and Emeis, K.-C.: Nutrient dynamics and oceanographic features in the central Namibian upwelling region as reflected in delta(15)N-signals of suspended matter and surface sediments, *Foss. Rec.*, 14, 153–169, doi:10.1002/mmng.201100005, 2011.
- Meyer, I., Davies, G. R., and Stuut, J.-B. W.: Grain size control on Sr-Nd isotope provenance studies and impact on paleoclimate reconstructions: An example from

## Holocene climate variability in the Winter Rainfall Zone of South Africa

S. Weldeab et al.

[Title Page](#)

[Abstract](#)

[Introduction](#)

[Conclusions](#)

[References](#)

[Tables](#)

[Figures](#)

[⏪](#)

[⏩](#)

[◀](#)

[▶](#)

[Back](#)

[Close](#)

[Full Screen / Esc](#)

[Printer-friendly Version](#)

[Interactive Discussion](#)

deep-sea sediments offshore NW Africa, *Geochem. Geophys. Geosyst.*, 12, Q03005, doi:10.1029/2010gc003355, 2011.

Miller, G. H., Geirsdottir, A., Zhong, Y., Larsen, D. J., Otto-Bliesner, B. L., Holland, M. M., Bailey, D. A., Refsnider, K. A., Lehman, S. J., Southon, J. R., Anderson, C., Björnsson, H., and Thordarson, T.: Abrupt onset of the Little Ice Age triggered by volcanism and sustained by sea-ice/ocean feedbacks, *Geophys. Res. Lett.*, 39, L02708, doi:10.1029/2011GL050168, 2012.

Moreno, P. I., Francois, J. P., Moy, C. M., and Villa-Martinez, R.: Covariability of the Southern Westerlies and atmospheric CO<sub>2</sub> during the Holocene, *Geology*, 38, 727–730, doi:10.1130/g30962.1, 2010.

Moy, C. M., Dunbar, R. B., Moreno, P. I., Francois, J. P., Villa-Martinez, R., Mucciarone, D. M., Guilderson, T. P., and Garreaud, R. D.: Isotopic evidence for hydrologic change related to the westerlies in SW Patagonia, Chile, during the last millennium, *Quaternary Sci. Rev.*, 27, 1335–1349, doi:10.1016/j.quascirev.2008.03.006, 2008.

Neumann, F. H., Scott, L., Bousman, C. B., and van As, L.: A Holocene sequence of vegetation change at Lake Eteza, coastal KwaZulu-Natal, South Africa, *Rev. Palaeobot. Palyno.*, 162, 39–53, doi:10.1016/j.revpalbo.2010.05.001, 2010.

Peeters, F. J. C., Acheson, R., Brummer, G. J. A., de Ruijter, W. P. M., Schneider, R. R., Ganssen, G. M., Ufkes, E., and Kroon, D.: Vigorous exchange between the Indian and Atlantic oceans at the end of the past five glacial periods, *Nature*, 430, 661–665, doi:10.1038/nature02785, 2004.

Prins, M., Postma, G., and Weltje, G. J.: Controls on terrigenous sediment supply to the Arabian Sea during the late Quaternary: the Makran continental slope, *Mar. Geol.*, 169, 351–371, doi:10.1016/s0025-3227(00)00087-6, 2000.

Prospero, J. M., Ginoux, P., Torres, O., Nicholson, S. E., and Gill, T. E.: Environmental characterization of global sources of atmospheric soil dust identified with the NIMBUS 7 Total Ozone Mapping Spectrometer (TOMS) absorbing aerosol product, *Rev. Geophys.*, 40, 1002, doi:10.1029/2000rg000095, 2002.

Reimer, P. J., Baillie, M. G. L., Bard, E., Bayliss, A., Beck, J. W., Blackwell, P. G., Ramsey, C. B., Buck, C. E., Burr, G. S., Edwards, R. L., Friedrich, M., Grootes, P. M., Guilderson, T. P., Hajdas, I., Heaton, T. J., Hogg, A. G., Hughen, K. A., Kaiser, K. F., Kromer, B., McCormac, F. G., Manning, S. W., Reimer, R. W., Richards, D. A., Southon, J. R., Talamo, S., Turney, C.

## Holocene climate variability in the Winter Rainfall Zone of South Africa

S. Weldeab et al.

[Title Page](#)

[Abstract](#)

[Introduction](#)

[Conclusions](#)

[References](#)

[Tables](#)

[Figures](#)

[⏪](#)

[⏩](#)

[◀](#)

[▶](#)

[Back](#)

[Close](#)

[Full Screen / Esc](#)

[Printer-friendly Version](#)

[Interactive Discussion](#)

- S. M., van der Plicht, J., and Weyhenmeyer, C. E.: Intcal09 and Marine09 radiocarbon age calibration curves, 0–50,000 years cal BP, *Radiocarbon*, 51, 1111–1150, 2009.
- Roethlisberger, R., Mulvaney, R., Wolff, E. W., Hutterli, M. A., Bigler, M., Sommer, S., and Jouzel, J.: Dust and sea salt variability in central East Antarctica (Dome C) over the last 45 kyr and its implications for southern high-latitude climate, *Geophys. Res. Lett.*, 29, 1963, doi:10.1029/2002gl015186, 2002.
- Rogers, J. and Rau, A. J.: Surficial sediments of the wave-dominated Orange River Delta and the adjacent continental margin off south-western Africa, *Afr. J. Mar. Sci.*, 28, 511–524, doi:10.2989/18142320609504202, 2006.
- Schaefer, J. M., Denton, G. H., Kaplan, M., Putnam, A., Finkel, R. C., Barrell, D. J. A., Andersen, B. G., Schwartz, R., Mackintosh, A., Chinn, T., and Schivöchter, C.: High-Frequency Holocene Glacier Fluctuations in New Zealand Differ from the Northern Signature, *Science*, 324, 622–625, doi:10.1126/science.1169312, 2009.
- Scott, L. and Woodborne, S.: Vegetation history inferred from pollen in Late Quaternary faecal deposits (hyraceum) in the Cape winter-rain region and its bearing on past climates in South Africa, *Quaternary Sci. Rev.*, 26, 941–953, doi:10.1016/j.quascirev.2006.12.012, 2007a.
- Scott, L. and Woodborne, S.: Pollen analysis and dating of Late Quaternary faecal deposits (hyraceum) in the Cederberg, Western Cape, South Africa, *Rev. Palaeobot. Palynol.*, 144, 123–134, doi:10.1016/j.revpalbo.2006.07.004, 2007b.
- Scott, L., Holmgren, K., and Partridge, T. C.: Reconciliation of vegetation and climatic interpretations of pollen profiles and other regional records from the last 60 thousand years in the Savanna Biome of Southern Africa, *Palaeogeogr. Palaeoclimatol.*, 257, 198–206, 2008.
- Scott, L., Neumann, F. H., Brook, G. A., Bousman, C. B., Norström, E., and Metwally, A. A.: Terrestrial fossil-pollen evidence of climate change during the last 26 thousand years in Southern Africa, *Quaternary Sci. Rev.*, 32, 100–118, doi:10.1016/j.quascirev.2011.11.010, 2012.
- Sealy, J., Dewar, G., and Reimer, P. J.: *S. Afr. J. Sci.*, in preparation, 2013.
- Shannon, L. V. and Anderson, F. P.: Applications of satellite ocean colour imagery in the study of the Benguela Current System, *The South African Journal of Photogrammetry, Remote Sensing and Cartography*, 13, 153–169, 1982.
- Shannon, L. V., Agenbag, J. J., Walker, N. D., and Lutjeharms, J. R. E.: A major perturbation in the Agulhas retroflection area in 1986, *Deep Sea Res. Part A. Oceanographic Research Papers*, 37, 493–512, doi:10.1016/0198-0149(90)90021-m, 1990.

## Holocene climate variability in the Winter Rainfall Zone of South Africa

S. Weldeab et al.

[Title Page](#)

[Abstract](#)

[Introduction](#)

[Conclusions](#)

[References](#)

[Tables](#)

[Figures](#)

[⏪](#)

[⏩](#)

[◀](#)

[▶](#)

[Back](#)

[Close](#)

[Full Screen / Esc](#)

[Printer-friendly Version](#)

[Interactive Discussion](#)



Shi, N., Dupont, L. M., Beug, H.-J. R., and Schneider, R.: Correlation between Vegetation in Southwestern Africa and Oceanic Upwelling in the Past 21,000 Years, *Quaternary Res.*, 54, 72–80, 2000.

5 Stager, J. C., Mayewski, P. A., White, J., Chase, B. M., Neumann, F. H., Meadows, M. E., King, C. D., and Dixon, D. A.: Precipitation variability in the winter rainfall zone of South Africa during the last 1400 yr linked to the austral westerlies, *Clim. Past*, 8, 877–887, doi:10.5194/cp-8-877-2012, 2012.

Stine, S. and Stine, M.: A record from Lake Cardiel Of climate change in southern South-America, *Nature*, 345, 705–708, doi:10.1038/345705a0, 1990.

10 Stuiver, M. and Reimer, P. J.: Extended 14C data-base and revised calib 3.0 C-14 age calibration program, *Radiocarbon*, 35, 215–230, 1993.

Stuut, J. B. W. and Lamy, F.: Climate variability at the southern boundaries of the Namib (South-western Africa) and Atacama (northern Chile) coastal deserts during the last 120,000 yr, *Quaternary Res.*, 62, 301–309, doi:10.1016/j.yqres.2004.08.001, 2004.

15 Stuut, J.-B. W., Prins, M. A., Schneider, R. R., Weltje, G. J., Jansen, J. H. F., and Postma, G.: A 300-kyr record of aridity and wind strength in southwestern Africa: inferences from grain-size distributions of sediments on Walvis Ridge, SE Atlantic, *Mar. Geol.*, 180, 221–233, 2002.

Toggweiler, J. R. and Lea, D. W.: Temperature differences between the hemispheres and ice age climate variability, *Paleoceanography*, 25, PA2212, doi:10.1029/2009pa001758, 2011.

20 Toggweiler, J. R., Russell, J. L., and Carson, S. R.: Midlatitude westerlies, atmospheric CO<sub>2</sub>, and climate change during the ice ages, *Paleoceanography*, 21, PA2005, doi:10.1029/2005PA001154, 2006.

Tyson, P. D., Karlen, W., Holmgren, K., and Heiss, G. A.: The Little Ice Age and medieval warming in South Africa, *S. Afr. J. Sci.*, 96, 121–126, 2000.

25 Tyson, P. D., Lee-Thorp, J., Holmgren, K., and Thackeray, J. F.: Changing gradients of climate change in Southern Africa during the past millennium: Implications for population movements, *Climatic Change*, 52, 129–135, doi:10.1023/a:1013099104598, 2002.

Vogel, J. C., Fuls, A., and Visser, E.: Radiocarbon adjustments to the dendrochronology of a yellowwood tree, *S. Afr. J. Sci.*, 97, 164–166, 2001.

30 Weldeab, S., Emeis, K.-C., Hemleben, C., Schulz, H., and Vennemann, T. W.: Sr, Nd isotope composition of Late Pleistocene sapropels and non-sapropel sediments from the Eastern Mediterranean Sea: Implications for detrital influx and climatic conditions in the source areas, *Geochim. Cosmochim. Acta*, 66, 3585–3598, 2002a.

Weldeab, S., Emeis, K.-C., Hemleben, C., and Siebel, W.: Provenance of lithogenic surface sediments and path ways of riverine suspended matters in the Eastern Mediterranean Sea: Evidence from  $^{143}\text{Nd}/^{144}\text{Nd}$  and  $^{87}\text{Sr}/^{86}\text{Sr}$  ratios, *Chem. Geol.*, 186, 139–149, 2002b.

5 Weldeab, S., Frank, M., Stichel, T., Haley, B., and Sungen, M.: Spatio-temporal evolution of the West African monsoon during the last deglaciation, *Geophys. Res. Lett.*, 38, L13703, doi:10.1029/2011gl047805, 2011.

Weltje, G. J.: End-member modeling of compositional data: Numerical-statistical algorithms for solving the explicit mixing problem, *Mathematical Geology*, 29, 503–549, doi:10.1007/bf02775085, 1997.

CPD

9, 2309–2356, 2013

## Holocene climate variability in the Winter Rainfall Zone of South Africa

S. Weldeab et al.

Title Page

Abstract

Introduction

Conclusions

References

Tables

Figures

⏪

⏩

◀

▶

Back

Close

Full Screen / Esc

Printer-friendly Version

Interactive Discussion



## Holocene climate variability in the Winter Rainfall Zone of South Africa

S. Weldeab et al.

**Table 1.** Details of the material used to establish an age model for GeoB8332-4.  $^{14}\text{C}$  ages were converted to calendar ages using CALIB software (Stuiver and Reimer, 1993) (version 6.10), Marine data set 2009 (Reimer et al., 2009), and  $\Delta R$  of  $129 \pm 19$  based on reservoir age of southeastern Atlantic water (Sealy et al. in preparation, data retrieved from <http://calib.qub.ac.uk/marine> as of 5 May 2012). The final age models were established using polynomial (11 500–5000 yr BP) and linear (0–700 yr BP) equations.

| Lab Code | Core       | core depth (cm) | Material  | 14C age yr BP    | Cal age yr BP (median probability) | 95.4 % ( $2\sigma$ ) cal age (yr BP) ranges | relative area under distribution | Calibration data     |
|----------|------------|-----------------|-----------|------------------|------------------------------------|---|----------------------------------|----------------------|
| KIA24630 | GeoB8332-4 | 2               | gastroods | $-220 \pm 30$    | 0                                  | 0   |                                  | Reimer et al. (2009) |
| KIA25048 | GeoB8332-4 | 50              | gastroods | $710 \pm 25$     | 219                                | 124–291                                     | 1                                | Reimer et al. (2009) |
| KIA25049 | GeoB8332-4 | 145             | gastroods | $1295 \pm 30$    | 709                                | 647–784                                     | 1                                | Reimer et al. (2009) |
| KIA25834 | GeoB8332-4 | 190             | gastroods | $4910 \pm 35$    | 5049                               | 4896–5229                                   | 1                                | Reimer et al. (2009) |
| KIA25833 | GeoB8332-4 | 220             | gastroods | $5290 \pm 35$    | 5525                               | 5438–5600                                   | 1                                | Reimer et al. (2009) |
| KIA25050 | GeoB8332-4 | 240             | gastroods | $5620 \pm 35$    | 5874                               | 5746–5965                                   | 1                                | Reimer et al. (2009) |
| KIA24623 | GeoB8332-4 | 319,5           | gastroods | $6730 \pm 90$    | 7115                               | 6888–7313                                   | 1                                | Reimer et al. (2009) |
| KIA25052 | GeoB8332-4 | 400             | gastroods | $7530 \pm 40$    | 7868                               | 7759–7927                                   | 1                                | Reimer et al. (2009) |
| KIA25053 | GeoB8332-4 | 489             | gastroods | $8625 \pm 40$    | 9121                               | 8999–9257                                   | 1                                | Reimer et al. (2009) |
| KIA25057 | GeoB8332-4 | 608             | gastroods | $9400 \pm 50$    | 10109                              | 9917–10217                                  | 1                                | Reimer et al. (2009) |
| KIA25056 | GeoB8332-4 | 699             | gastroods | $9840 \pm 50$    | 10568                              | 10466–10703                                 | 1                                | Reimer et al. (2009) |
| KIA25055 | GeoB8332-4 | 789             | gastroods | $10\,380 \pm 85$ | 11\,253                            | 11\,102–11\,445                             | 0.9                              | Reimer et al. (2009) |
|          |            |                 |           |                  |                                    | 11\,460–11\,630                             | 0.1                              | Reimer et al. (2009) |
| KIA24622 | GeoB8332-4 | 789,5           | gastroods | $10\,440 \pm 50$ | 11\,290                            | 11\,177–11\,428                             | 0.91                             | Reimer et al. (2009) |
|          |            |                 |           |                  |                                    | 11\,487–11\,617                             | 0.09                             | Reimer et al. (2009) |
| KIA25059 | GeoB8332-4 | 805             | gastroods | $10\,485 \pm 50$ | 11\,357                            | 11\,214–11\,649                             | 1                                | Reimer et al. (2009) |

Title Page

Abstract

Introduction

Conclusions

References

Tables

Figures

⏪

⏩

◀

▶

Back

Close

Full Screen / Esc

Printer-friendly Version

Interactive Discussion

## Holocene climate variability in the Winter Rainfall Zone of South Africa

S. Weldeab et al.

**Table 2.** Results of Sr and Nd isotope analysis in river and marine core sediments.

| River samples      |                              |                          |                           |               |                                 |                                    |                                   |                                      |        |               |
|--------------------|------------------------------|--------------------------|---------------------------|---------------|---------------------------------|------------------------------------|-----------------------------------|--------------------------------------|--------|---------------|
| Sample code        | Location                     | Locarion                 | Material                  | size fraction | $^{87}\text{Sr}/^{86}\text{Sr}$ | $\pm^{87}\text{Sr}/^{86}\text{Sr}$ | $^{143}\text{Nd}/^{144}\text{Nd}$ | $\pm^{143}\text{Nd}/^{144}\text{Nd}$ | eNd    | error eNd (2) |
| SP-B1              | Buffels River                | 29°41.97' S/17°42.75' E  | riverine mud              | < 125 µm      | 0.76760                         | 0.00001                            | 0.51170                           | 0.00001                              | -18,20 | 0,12          |
| SP-B2              | Buffels River                | 29°36.79' S/17°31.45' E  | riverine mud              | < 125 µm      | 0.75528                         | 0.00001                            | 0.51176                           | 0.00001                              | -17,05 | 0,12          |
| SP-FB              | Dry river bed                | 28°47.94' S/17°39.06' E  | riverine mud              | < 125 µm      | 0.76666                         | 0.00001                            | 0.51169                           | 0.00001                              | -18,41 | 0,12          |
| SP-OL              | Olifants Rivers              | 31° 40.76'S/18° 11.98'E  | riverine mud              | < 125 µm      | 0.72423                         | 0.00001                            | 0.51207                           | 0.00001                              | -11,12 | 0,12          |
| SP-H               | Hoigat River                 | 28°55.86' S/16°46.44' E  | riverine mud              | < 125 µm      | 0.72320                         | 0.00001                            | 0.51192                           | 0.00001                              | -13,97 | 0,12          |
| B005               | Orange River (Alexander Bay) | 28°36'07" S/16.28'16" E  | riverine mud              | > 2 µm        | 0.735538                        | 0.000001                           | 0.512032                          | 0.000007                             | -11,78 | 0,14          |
| SF-OR              | Orange River (Voolsdrif)     | 28°46'41" S/17°38'63"VE  | riverine suspended matter | < 20 µm       | 0.733628                        | 0.000001                           | 0.512015                          | 0.000007                             | -12,11 | 0,14          |
| "Alagae"           | Orange River (Voolsdrif)     | 28.36'07" S/16.28'16" E  | riverine suspended matter | > 2 µm        | 0.732447                        | 0.000001                           | 0.511991                          | 0.000009                             | -12,58 | 0,18          |
| SP-OR1             | Orange River (Voolsdrif)     | 28° 46'41" S/17° 38.63'E | riverine mud              | < 120 µm      | 0.727351                        | 0.000027                           | 0.511956                          | 0.000008                             | -13,26 | 0,16          |
| GeoB8332-4 samples |                              |                          |                           |               |                                 |                                    |                                   |                                      |        |               |
| core               | sediment depth (cm)          | cal. age (yr, BP)        | Material                  | size fraction | $^{87}\text{Sr}/^{86}\text{Sr}$ | $\pm^{87}\text{Sr}/^{86}\text{Sr}$ | $^{143}\text{Nd}/^{144}\text{Nd}$ | $\pm^{143}\text{Nd}/^{144}\text{Nd}$ | eNd    | error eNd (2) |
| GeoB8332-4         | 2                            | 0                        | Terrigenous fraction      | < 125 µm      | 0.734426                        | 0.000009                           | 0.512066                          | 0.000008                             | -11,12 | 0,16          |
| GeoB8332-4         | 35                           | 157,2                    | Terrigenous fraction      | < 125 µm      | 0.734077                        | 0.000008                           | 0.512081                          | 0.000009                             | -10,83 | 0,18          |
| GeoB8332-4         | 102,5                        | 493,6                    | Terrigenous fraction      | < 125 µm      | 0.729606                        | 0.000008                           | 0.512103                          | 0.000010                             | -10,40 | 0,20          |
| GeoB8332-4         | 180                          | 879,8                    | Terrigenous fraction      | < 125 µm      | 0.721613                        | 0.00001                            | 0.512047                          | 0.000007                             | -11,49 | 0,14          |
| GeoB8332-4         | 230                          | 5736,7                   | Terrigenous fraction      | < 125 µm      | 0.721173                        | 0.00001                            | 0.512052                          | 0.000010                             | -11,39 | 0,20          |
| GeoB8332-4         | 285                          | 6551,2                   | Terrigenous fraction      | < 125 µm      | 0.719441                        | 0.00001                            | 0.512045                          | 0.000009                             | -11,53 | 0,18          |
| GeoB8332-4         | 315                          | 6972,6                   | Terrigenous fraction      | < 125 µm      | 0.721116                        | 0.000009                           | 0.512049                          | 0.000010                             | -11,45 | 0,20          |
| GeoB8332-4         | 385                          | 7892,7                   | Terrigenous fraction      | < 125 µm      | 0.72176                         | 0.00001                            | 0.512064                          | 0.000010                             | -11,16 | 0,20          |
| GeoB8332-4         | 445                          | 8611,2                   | Terrigenous fraction      | < 125 µm      | 0.724198                        | 0.000007                           | 0.512047                          | 0.000010                             | -11,49 | 0,20          |
| GeoB8332-4         | 470                          | 8891,5                   | Terrigenous fraction      | < 125 µm      | 0.724615                        | 0.000009                           | 0.512047                          | 0.000007                             | -11,49 | 0,14          |
| GeoB8332-4         | 485                          | 9054,2                   | Terrigenous fraction      | < 125 µm      | 0.725862                        | 0.00001                            | 0.512034                          | 0.000009                             | -11,74 | 0,18          |
| GeoB8332-4         | 552,5                        | 9736,5                   | Terrigenous fraction      | < 125 µm      | 0.731262                        | 0.000008                           | 0.512051                          | 0.000009                             | -11,41 | 0,18          |
| GeoB8332-4         | 662,5                        | 10672,6                  | Terrigenous fraction      | < 125 µm      | 0.731666                        | 0.000009                           | 0.51206                           | 0.000009                             | -11,24 | 0,18          |
| GeoB8332-4         | 745                          | 11231,7                  | Terrigenous fraction      | < 125 µm      | 0.732319                        | 0.00001                            | 0.512082                          | 0.000009                             | -10,81 | 0,18          |
| GeoB8332-4         | 775                          | 11404,7                  | Terrigenous fraction      | < 125 µm      | 0.73493                         | 0.000008                           | 0.512074                          | 0.000005                             | -10,96 | 0,10          |

Title Page

Abstract

Introduction

Conclusions

References

Tables

Figures



Back

Close

Full Screen / Esc

Printer-friendly Version

Interactive Discussion



## Holocene climate variability in the Winter Rainfall Zone of South Africa

S. Weldeab et al.

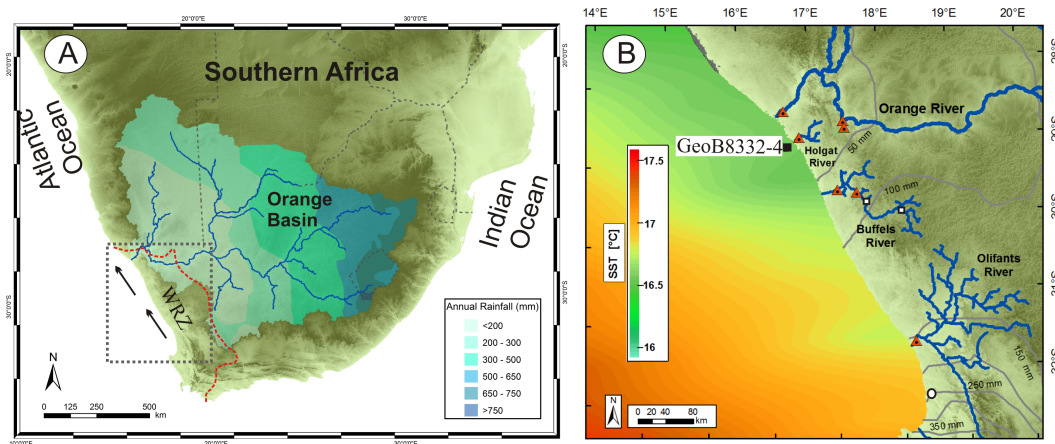


**Fig. 1. (A)** Map of southern Africa indicating the basin of the Orange River, annual rainfall over the basin (rainfall contour redrawn from Compton et al. (2010)), and the Winter Rainfall Zone (WRZ) delineated by the orange line. Black arrows indicate southeasterly trade winds. Dotted square indicate area whose details is shown **(B)**. **(B)** Coastal area of southwestern Africa showing local rivers, annual precipitation (gray contours), annual sea surface temperature (Locarnini et al., 2010), location of GeoB8332-4 (black square), and riverine sediment samples used for Sr and Nd isotope analyses (orange triangles). Shown is also the approximate location of Lake Verlorenvlei (white circle) (Stager et al., 2012) and paleo-flood investigation on the Buffels River banks (white squares) (Benito et al., 2011).

Title Page

Abstract

Introduction

Conclusions

References

Tables

Figures

⏪

⏩

◀

▶

Back

Close

Full Screen / Esc

Printer-friendly Version

Interactive Discussion

## Holocene climate variability in the Winter Rainfall Zone of South Africa

S. Weldeab et al.

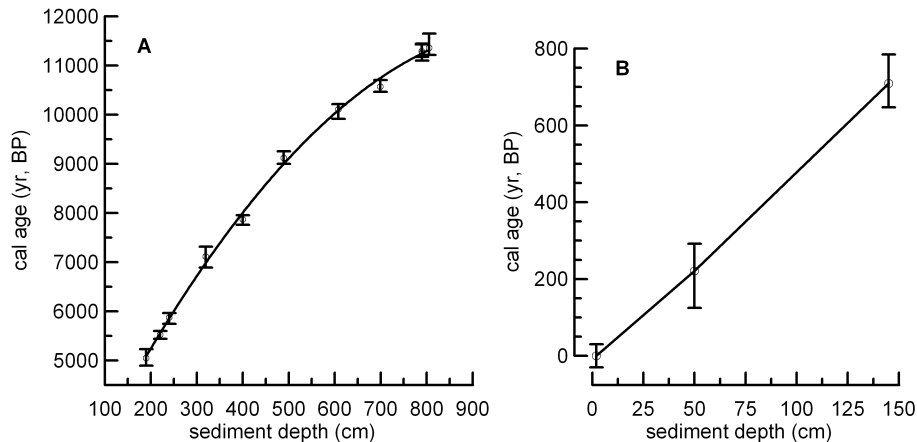


**Fig. 2.** Calendar age versus GeoB8332-1 sediment depth. Open circles, vertical bars, and lines indicate  $^{14}\text{C}$ -based age model control points, uncertainty in the age model control points ( $2\sigma$ ), and the final age model that is based on polynomial (A) and linear fits (B).

Title Page

Abstract

Introduction

Conclusions

References

Tables

Figures

◀

▶

◀

▶

Back

Close

Full Screen / Esc

Printer-friendly Version

Interactive Discussion

## Holocene climate variability in the Winter Rainfall Zone of South Africa

S. Weldeab et al.

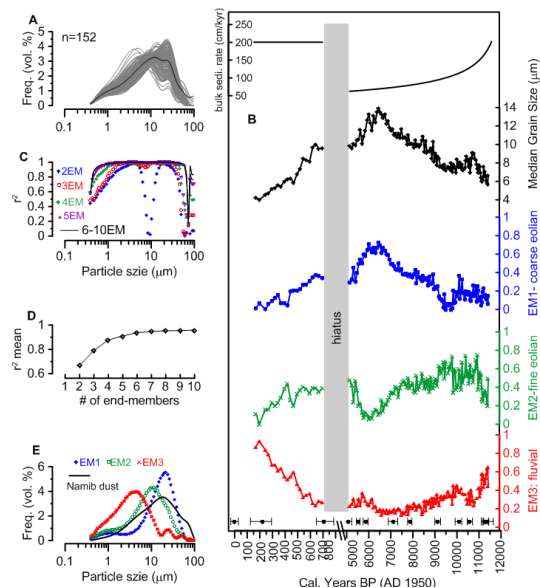


**Fig. 3.** Results of grain size analysis and end-member modeling for core GeoB8332-4 material. **(A)** Grain size distribution frequency for 152 samples (grey lines) and average grain size distribution frequency for the entire data set (black line). **(B)** Sedimentation rate of bulk sediment, temporal distribution of median grain size and modeled end-members 1–3, indicating coarse eolian (EM1), fine eolian (EM2), and fluvial (EM3) components. Black filled circles and horizontal bars indicate age model control points and error estimate ( $2\sigma$ ) obtained from  $^{14}\text{C}$  datings and conversion to calendar age. **(C)**  $r^2$  goodness-of-fit of models with 2–10 end-members for each particle size class. **(D)**  $r^2$  mean (mean coefficient of determination) of all size classes for each end-member model. **(E)** Comparison of particle size distributions in EM1, EM2, and EM3 with present-day dust collected over the Walvis Ridge (Stuut et al., 2002).

Title Page

Abstract Introduction

Conclusions References

Tables Figures

◀ ▶

◀ ▶

Back Close

Full Screen / Esc

Printer-friendly Version

Interactive Discussion

## Holocene climate variability in the Winter Rainfall Zone of South Africa

S. Weldeab et al.

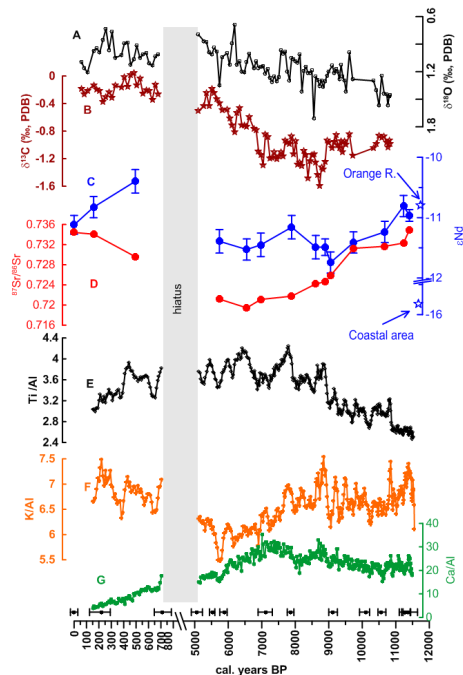


**Fig. 4.** Proxy time series analyzed in sediment core GeoB8332-4. **(A)** and **(B)**  $\delta^{18}\text{O}$  and  $\delta^{13}\text{C}$  analyzed in tests of *N. pachyderma* (sinistral). **(C)** and **(D)**  $\epsilon\text{Nd}$  and  $^{87}\text{Sr}/^{86}\text{Sr}$  analyzed in the detrital fraction. Average  $\epsilon\text{Nd}$  value of Orange River and river-bed sediments from the coastal area indicated by stars in the y-axis. Vertical bars indicate analytical error estimates for  $\epsilon\text{Nd}$ . Analytical error estimate for  $^{87}\text{Sr}/^{86}\text{Sr}$  is smaller than the dots indicating individual measurements. Ti/Al **(E)**, K/Al **(F)**, and Ca/Al **(G)** analyzed in bulk sediment of GeoB8332-4 using XRF-Scanning. Black filled circles and horizontal bars indicate age model control points and error estimate ( $2\sigma$ ) related to  $^{14}\text{C}$  measurements and conversion to calendar age, respectively.

Title Page

Abstract

Introduction

Conclusions

References

Tables

Figures

◀

▶

◀

▶

Back

Close

Full Screen / Esc

Printer-friendly Version

Interactive Discussion

## Holocene climate variability in the Winter Rainfall Zone of South Africa

S. Weldeab et al.

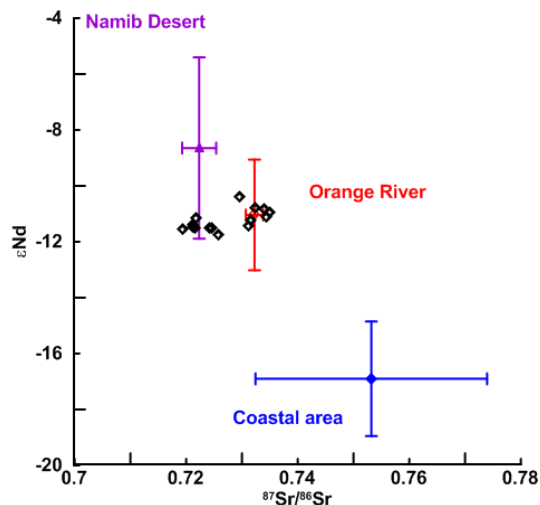


**Fig. 5.** Sr and Nd isotope signatures of the main sediment sources and temporal variation in sediment core GeoB8332-4 (open diamonds). Mean  $^{87}\text{Sr}/^{86}\text{Sr}$  and  $\epsilon\text{Nd}$  values and standard deviations of Namib Desert dust ( $^{87}\text{Sr}/^{86}\text{Sr}=0.722 \pm 0.003$  and  $\epsilon\text{Nd}=-8.65 \pm 3.24$ ,  $n = 6$ ) (Grousset et al., 1992), sediment of coastal area ( $^{87}\text{Sr}/^{86}\text{Sr}=0.75318 \pm 0.02$  and  $\epsilon\text{Nd} = -16.9 \pm 2.05$ ,  $n = 2$ ), Orange River sediments collected at Alexander Bay and Vioolsdrift (see Fig. 1) and main catchment of Orange River (Dia et al., 1990) ( $^{87}\text{Sr}/^{86}\text{Sr}=0.7322 \pm 0.0015$ ,  $n = 4$  and  $\epsilon\text{Nd}=-11.04 \pm 1.98$ ,  $n = 6$ ).

Title Page

Abstract

Introduction

Conclusions

References

Tables

Figures

⏪

⏩

◀

▶

Back

Close

Full Screen / Esc

Printer-friendly Version

Interactive Discussion



## Holocene climate variability in the Winter Rainfall Zone of South Africa

S. Weldeab et al.

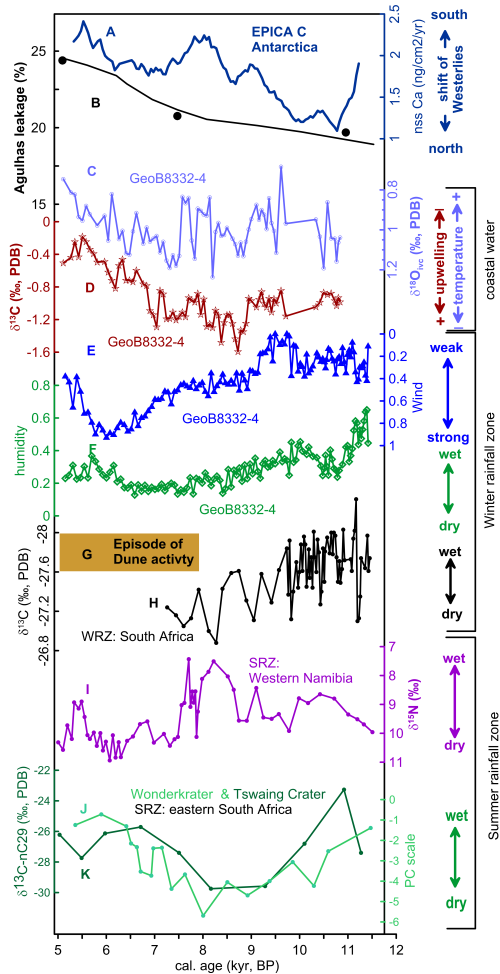


Fig. 6. Caption on next page.

Title Page

Abstract

Introduction

Conclusions

References

Tables

Figures

⏪

⏩

◀

▶

Back

Close

Full Screen / Esc

Printer-friendly Version

Interactive Discussion



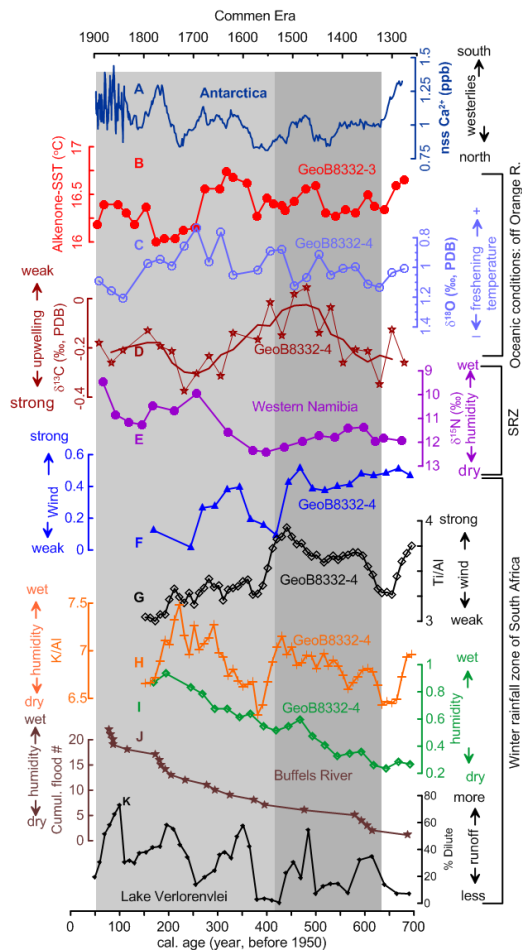


Fig. 7. Caption on next page.

## Holocene climate variability in the Winter Rainfall Zone of South Africa

S. Weldeab et al.

[Title Page](#)

[Abstract](#) | [Introduction](#)

[Conclusions](#) | [References](#)

[Tables](#) | [Figures](#)

[◀](#) | [▶](#)

[◀](#) | [▶](#)

[Back](#) | [Close](#)

[Full Screen / Esc](#)

[Printer-friendly Version](#)

[Interactive Discussion](#)

## Holocene climate variability in the Winter Rainfall Zone of South Africa

S. Weldeab et al.

**Fig. 7.** Environmental conditions during the “Little Ice Age” in southwestern Africa. **(A)** 21-points running average of non-sea-salt  $\text{Ca}^{2+}$  ( $\text{nss Ca}^{2+} = \text{Na} - 0.038 * \text{Ca}^{2+}$ ) analyzed in Antarctic ice core (Siple Dom) (Kreutz and Mayewski, 1999). **(B)** Alkenone-based SST estimates off Holgat River analyzed in GeoB8332-3 (Leduc et al., 2010). Note that the locations of GeoB8332-3 and GeoB8332-4 are identical. **(C)**  $\delta^{18}\text{O}$  and **(D)**  $\delta^{13}\text{C}$  analyzed in *N. pachyderma* (sinistral) in core GeoB8332-4. **(E)**  $\delta^{15}\text{N}$  analyzed in hyrax dung from the SRZ in western Namibia (Chase et al., 2009). **(F)** Wind strength inferred from grain size analyses and modeling in core GeoB8332-4. **(G)** Ti/Al and **(H)** K/Al analyzed in core GeoB8332-4. **(I)** Humidity index inferred from grain size analyses and modeling in core GeoB8332-4. **(J)** Cumulative flood number over the last 700 years BP reconstructed in Buffels River banks (Benito et al., 2011). **(K)** Percentage of diatom assemblages that are indicative for enhanced runoff in Lake Verlorenvlei (Stager et al., 2012). Dark grey area indicates time interval when fluvial proxies suggest wet conditions, high dust input, and strong winds in the WRZ. Light grey area indicates episode of wet conditions in both WRZ and SRZ.

Title Page

Abstract

Introduction

Conclusions

References

Tables

Figures

⏪

⏩

◀

▶

Back

Close

Full Screen / Esc

Printer-friendly Version

Interactive Discussion